An Experimentally Validated Model of the Propeller Force Accounting for Cross Influences on Multi-Rotor Aerial Systems

Barbara Bazzana*, Ralph Brantjes*, Chiara Gabellieri*, and Antonio Franchi*,†

***Abstract*— In this paper, we propose a model for the thrust coefficient of propellers that can take into account cross-influence between adjacent propellers. The aerodynamic interaction between propellers in multirotor aerial vehicles reduces the thrust they can produce. The influence between propellers depends on their relative positioning and orientation, which are taken into account by the proposed model. It is validated on measurements collected by a force sensor mounted on a propeller for different configurations of the adjacent propellers in a support structure. In this work, we focus on configurations with small relative orientations. Results show that the proposed model outperforms the traditional constant model in terms of thrust prediction on the data we collected, and it performs better than other models with fewer parameters, being the only one with less than 10% maximum percentage error.**

I. Introduction

The design of multirotor aerial vehicles evolved in the recent years to improve their actuation properties [1]. Omnidirectional platforms can be obtained by tilting the propellers [2], [3]. Hovering in the presence of propeller failures can be achieved with alternative designs, e.g. with a Y-shaped propeller instead of the traditional star-shaped [4], [5].

At the same time, the literature has shown a trade-off between actuation capabilities and robustness on one side and energy efficiency on the other. The most efficient configurations are the ones with collinear propellers, however, it is not the one that allows to achieve omnidirectionality. This is the reason why omnidirectional designs with actively tilting propellers have gained attention [6], [7].

Simplistic models assume that the force generated by a propeller depends only on the rotational speed of the propeller, see e.g., [8]. Those models work well for collinear propeller platforms, however, they produce an unsatisfactory prediction of the actual force produced by the propeller in omnidirectional and fully actuated platforms. In those platforms, the presence of non-collinear propellers generates mutual influences between the propellers. The airflow produced by adjacent propellers influences the force that a propeller generates. To cope with such a shortcoming we propose a model of the force of the propeller that includes as inputs both the angular velocity of the propeller and the angular velocities and the relative poses of the other propellers.

The new model is the result of an analysis of the physical characteristics of the interaction on configurations with small relative orientations between propellers ($< 10°$). The proposed model can give satisfactory predictions of the force produced by a rotor, with mean percentage error below 5% and maximum percentage error below 10%. This comes at the price of having four parameters instead of just one. We can show that the same error requirements cannot be satisfied by models with fewer parameters.

The validation has been carried out on force measurements collected on a propeller mounted on a structure that allows the placement of up to eight propellers and can be modified to change their mutual position. The experimental data are symmetrically split into two sets: one that is used to estimate the parameters by solving a least squares problem, and one that is used for testing their efficacy in predicting the measured force.

Summarizing, this work introduces a novel model of the thrust coefficient of a propeller that can take into account cross-influence effects. It trades off the complexity and descriptivity of the phenomena, as it can satisfactorily predict the measured force at the price of an increased number of parameters on the data we collected. Future work includes extension to general relative orientations of the propellers.

II. Related Work

Micro Aerial Vehicle (MAV) designs provide them with different actuation properties, such as omnidirectionality, static hovering in the presence of disturbance, and force-moment decoupling. Michieletto *et al.* [4] deeply analyzed statically hovering in case of propeller failures and force-moment decoupling, through algebraic conditions on the control allocation matrices. This allowed them to show that a Y-shaped hexarotor is more robust than a star-shaped one with collinear propellers.

Baskaya *et al.* [5] further investigated static hovering in the presence of propeller failures. They provided an efficiency analysis to better draw the advantages and disadvantages of the possible configurations and highlight that the initial

* Robotics and Mechatronics Department, Electrical Engineering, Mathematics, and Computer Science (EEMCS) Faculty, University of Twente, 7500 AE Enschede, The Netherlands. b.bazzana@utwente.nl, r.j.brantjes@student.utwente.nl, c.gabellieri@utwente.nl, a.franchi@utwente.nl

† Department of Computer, Control and Management Engineering, Sapienza University of Rome, 00185 Rome, Italy, antonio.franchi@uniroma1.it

This work was partially funded by the Horizon Europe research and innovation programs under agreement no. 101059875 (FlyFlic) and agreement no. 101120732 (AUTOASSESS).

voltage drop of the Y-shaped hexarotor is higher than that of the star-shaped one. Their intuition was that the interaction between co-axial propellers reduces their efficiency. In this work, we design an extended model of the thrust coefficient that is suitable for modeling cross-influence between propellers.

Recently, several works addressed the design of omnidirectional multirotors as they are crucial in achieving specific application tasks. Omnidirectionality has been achieved in mainly three ways: using fixedly tilted bidirectional propellers [2], [9], [3], optimizing the orientation of fixedly tilted unidirectional propellers [10], and actively tilting uni- and bi-directional propellers [11], [12], [7]. A relevant property for aerial platforms is being designed to be energy-efficient, because of the limited flight endurance. The third choice is the most suitable in this sense because propellers can be aligned in such a way to maximize the efficiency when the full actuation capacity is not needed [6]. The model we propose here allows predicting the loss in efficiency of the single propellers given its relative pose and angular velocity with respect to the others.

To the best of our knowledge, the aerodynamic interaction between the propellers of a UAV has not been investigated so far, to provide an extended model of the thrust coefficient. State-of-the-art papers consider large propulsion systems [13] or laterally spaced propellers with no overlap between blade areas [14]. Differently from us, they conduct wind tunnel experiments. We propose an experimentally validated model of the thrust coefficient that embeds the cross-influence by adding configuration-dependent terms to the influence-free constant thrust coefficient.

III. Methodology

In a multi-rotor structure, each propeller produces a thrust force $\mathbf{f}_i \in \mathbb{R}^3$, typically modeled in the literature as [6]:

$$\mathbf{f}_i = k_i c_{f,0} w_i |w_i| \mathbf{z}_i. \tag{1}$$

where $c_{f,0} > 0$ is a constant thrust coefficient, $\mathbf{z}_i$ is the z-axis of the propeller frame, w_i is the intensity of the propeller angular velocity $\boldsymbol{\omega}_i$ with positive sign when $\mathbf{z}_i$ and $\boldsymbol{\omega}_i$ have the same direction and negative sign otherwise, and k_i is a number defined as $k_i = 1$ for propellers with descending chords and $k_i = -1$ for propellers with ascending chords. However, the approximation with constant $c_{f,0}$ may be not satisfactory in the presence of mutual interaction between the propellers. It does not model the effect on the thrust produced by a propeller when it is influenced by the airflow of the adjacent ones. Fig. 1 and 2 give an intuition of the physics: the actuation of propeller j produces an airflow that reduces the thrust effectiveness of propeller i. The effect depends on the mutual positioning, orientation, and spinning rate of the propellers. These quantities can be codified by mathematical expressions involving: the relative position vector $\mathbf{p}_{ij}$ of the propellers and their angular velocities $\boldsymbol{\omega}_i$ and $\boldsymbol{\omega}_j$.

Let us introduce the following notations:

- N the total number of propellers
- $c_{f,0}$ the thrust coefficient without cross-influence

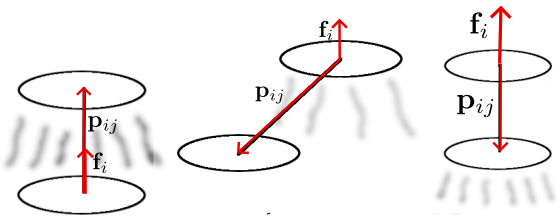

Fig. 1. Visual intuition of the cross-influence due to the angle between relative position $\mathbf{p}_{ij}$ and thrust force $\mathbf{f}_i$ on propeller i. Independently of the propeller's type, the propeller is maximally affected when $\mathbf{p}_{ij}$ and $\mathbf{f}_i$ are aligned, and not affected at all when they have opposite directions.

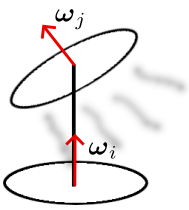

Fig. 2. Visual intuition of the cross-influence due to the angle between the angular velocities w_i and w_j on propeller i. The propeller is maximally affected when the two vectors are aligned. This effect decreases as the angle approaches $90°$

- $p_{ij} = ||\mathbf{p}_{ij}||$ the norm of $\mathbf{p}_{ij}$
- $\theta_{p,ij} = \widehat{\mathbf{p}_{ij}, \mathbf{f}_i}$ the angle between $\mathbf{p}_{ij}$ and the thrust force $\mathbf{f}_i$ of propeller i
- $\theta_{w,ij} = \widehat{\boldsymbol{\omega}_i, \boldsymbol{\omega}_j}$ the angle between $\boldsymbol{\omega}_i$ and $\boldsymbol{\omega}_j$

and group the kinematic parameters using the symbol $\boldsymbol{\gamma}_i = \{p_{ij}, \theta_{w,ij}, \theta_{w,ij}, j = 1, ..., N\}$. We propose to replace the constant thrust coefficient $c_{f,0}$ with a more complex one $c_{f,i}(w_{1:N}, \boldsymbol{\gamma}_i, \mathbf{x})$ depending on the time-varying angular velocity rates $w_{1:N}$, the kinematic parameters $\boldsymbol{\gamma}$ which we assume constant for a given setup, and a set of data fitting parameters $\mathbf{x}$. The thrust force of (1) becomes

$$\mathbf{f}_i = c_{f,i}(w_{1:N}, \boldsymbol{\gamma}_i, \mathbf{x}) w_i |w_i| \mathbf{z}_i. \tag{2}$$

where the dependence on the angular velocity of propeller i is in general nonlinear, rather than quadratic as in state-of-the-art models. The model in (2) boils down to (1) when all the data fitting parameters $\mathbf{x}$ are set to zero.

Many models could be envisioned for $c_{f,i}$. In this work we propose the following model:

$$\begin{aligned} c_{f,i}(w_{1:N}, \boldsymbol{\gamma}_i, \mathbf{x}) = c_{f,0} - \sum_{j=1:N, j\neq i} \frac{|w_j|^2}{|w_i|} \Bigg[x_1 \frac{1}{p_{ij}} + \\ + x_2 \cos\left(\frac{1}{2}\theta_{p,ij}\right) \frac{1}{p_{ij}} + \\ + x_3 \cos\left(\frac{1}{2}\theta_{p,ij}\right) \cos^2\left(\theta_{w,ij}\right) \Bigg] \end{aligned} \tag{3}$$

Despite its apparent complexity, the model is fully described by only four parameters $c_{f,0}, x_{1:3} \in \mathbb{R}$ that can be determined from experimental data. It introduces the dependency on the angular spinning rate $w_{1:N}$ and the propellers configuration $\boldsymbol{\gamma}_i$ to capture the cross-influence effects. In this way, we have traded off the complexity and descriptivity of the physical phenomena. Notice that (3) does not guarantee

that $c_{f,i}(w_{1:N}, \boldsymbol{\gamma}_i, \mathbf{x}) > 0$, which is the set of physically meaningful values. At the same time, we show here that the model is both simple and effective in the domain of validity that we have explored. We leave as future work modifications of (2) to make the thrust coefficient positive by construction.

In the following, we motivate in detail each term in (3). The first term handles the distance between the two propellers and the ratio between the angular velocities. The farther the propellers, the lower the cross-influence. Also, if propeller j is not spinning, i.e., $w_j = 0$, it should not affect propeller i at all. The faster it spins, the more intense the airflow affecting propeller i. At the same time, the larger the angular velocity of i the smaller the effect of another spinning propeller on it. The corresponding term in (1) is weighted by the data fitting coefficient x_1, whose measurement unit is $\mathrm{N} \cdot \mathrm{s}^3/\mathrm{m}$, accounting for the nonlinear dependence on the angular spinning rates and the inverse of the distance between the coefficients.

The second term accounts for the fact that propeller i is affected only by airflow in the semi-space to which the thrust vector belongs. Fig. 1 illustrates three possible configurations: the one with the thrust $\mathbf{f}_i$ parallel to $\mathbf{p}_{ij}$ giving the maximum cross-influence, the one with a non-zero angle between $\mathbf{f}_i$ and $\mathbf{p}_{ij}$ giving medium influence, finally the one with $\mathbf{f}_i$ anti-parallel to $\mathbf{p}_{ij}$, where propeller i is not even affected by propeller j below. The data fitting coefficient x_2 has also measurement unit $\mathrm{N} \cdot \mathrm{s}^3/\mathrm{m}$ because the only difference between the first and the second term in (3) is in the space information encoded in $\cos(\theta_{p,ij}/2)$, which is dimensionless.

The third term in the summation (3) accounts also for the relative orientation between propellers. Even in the case where $\mathbf{p}_{ij}$ is perfectly aligned with $\mathbf{f}_i$, it can still be the case that propeller j is tilted as in Fig. 2, giving a non-zero $\theta_{w,ij}$: the larger the angle, the smaller the cross-influence. At the same time, if propeller i is on top of propeller j it will not be influenced by propeller j whatever the angle is between the two angular velocities. This explains the factor depending on $\theta_{p,ij}$. Notice that, in general, $\theta_{p,ij} \neq \theta_{w,ij}$. Only propellers that rotate counterclockwise have thrust parallel to the angular velocity pointing upwards. The data fitting coefficient x_3 has measurement unit $\mathrm{N} \cdot \mathrm{s}^3$, as the third term does not depend on the distance as the other two.

Summarizing, compared to the constant thrust coefficient of the traditional model (1), the coefficient we propose involves four data fitting parameters: the influence-free thrust coefficient $c_{f,0}$, and the three weights x_1, x_2, x_3. This allows us to model the cross-influence interaction with adjacent propellers, that is crucial to improve the prediction of the force generated by the rotors in a MAVs. We validated the model on experimental data as we detail in the following.

IV. Experimental validation

The experimental set-up consists of the structure in Fig. 3 that allows the placement and orientation of several propellers, up to eight. We have mounted propellers with brushless motors: alternating counterclockwise- and clockwise-rotating. The two propellers on top of each other are always of the same type. Based on the physical intuition presented before, the propellers at the bottom are the most affected by cross-influence with the surroundings, so we have placed a force sensor on one of the bottom propellers. In the following, we describe the three families of configurations considered.

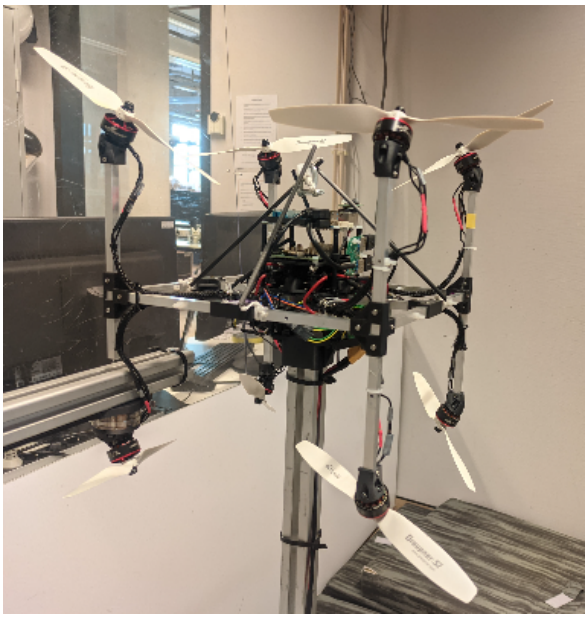

Fig. 3. Experimental set-up.

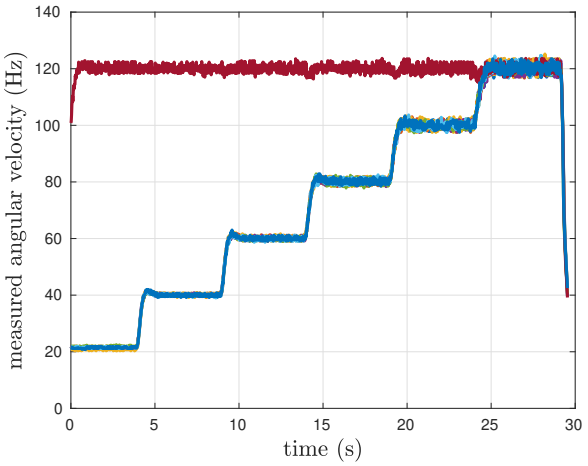

Fig. 4. Measured angular velocity for experimental set-up in Fig. 3 with all rotors spinning. The velocity of the measured propeller is in red.

The first experimental setting aims to show the different impacts of the adjacent propellers depending on the alignment between thrust and relative positioning. To do this, we have collected force data on the measured propellers in four scenarios: (a) only the measured propeller is spinning; (b) all the eight propellers are spinning (see Fig. 4); (c) seven propellers are spinning, all of them but the one above the measured propeller (see Fig. 5); (d) only the measured propeller and the one on top of it are spinning (see Fig. 6).

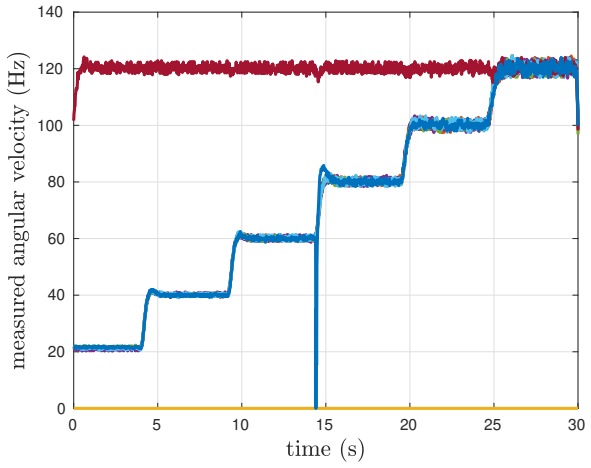

Fig. 5. Measured angular velocity for experimental set-up in Fig. 3 with all rotors but the one above the measured propeller spinning. The velocity of the measured propeller is in red. The yellow line at zero is the velocity of the propeller right above it.

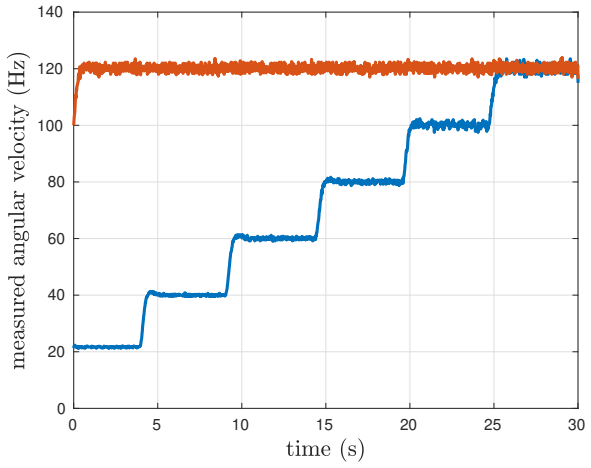

Fig. 6. Measured angular velocity for experimental set-up in Fig. 3 with only the measured propeller and the one above spinning. The red signal corresponds to the measured propeller; the blue one to the propeller above.

We have collected measurements for various spinning rates of the non-measured propellers, to be able to observe the dependence on the relative spinning rate of the rotors. In particular, for each of the configurations (b), (c) and (d) we have collected data for six different angular velocity values as illustrated in the pictures.

Fig. 7 illustrates the force on the measured propellers in the four scenarios (a)-(d). The largest value of the force is obtained without cross-influence. At the same time, the cross-influence of the propeller above is predominant compared to that of all the other propellers. Indeed, the red curve, representing the two-propeller scenario (d), is already a good approximation of the purple curve, representing the experiment with all the propellers spinning—scenario (b). The loss in the thrust force of the measured propeller is way lower when seven propellers are spinning, but not the one above the measured one—scenario (c). These experimental data confirm the intuition that the maximum loss in force

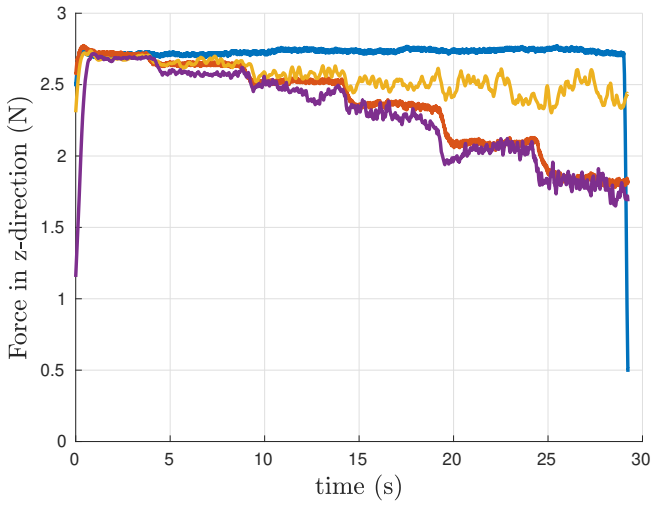

Fig. 7. Measured force in the first experimental setting: without cross-influence (blue), all propellers spinning (purple), only the propeller on top of the measured one spinning (red), all the propellers but the one on top (yellow).

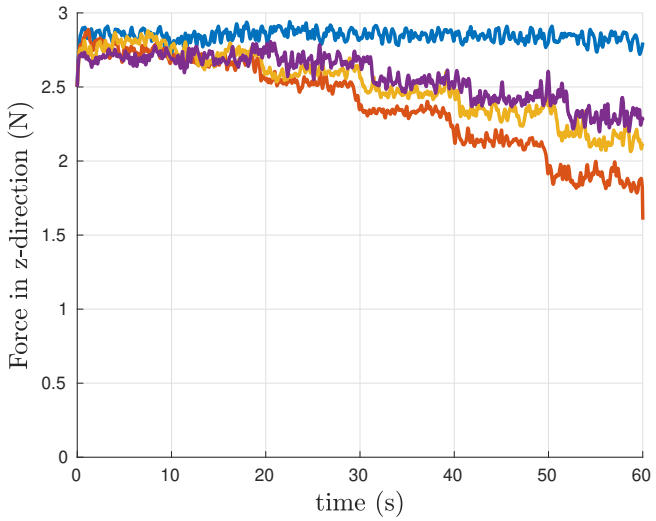

Fig. 8. Measured force in the second experimental setting: only the measured propeller and the one above are spinning. The data correspond to different distances between the two propellers: 14 cm (red), 34 cm (yellow), 54 cm (purple). The blue plot corresponds to the force without cross-influence.

occurs when the thrust and the relative position vectors are aligned. The worst case is therefore having a propeller on top.

The second experimental setting is designed to observe the impact of the distance between cross-influencing propellers. Only the measured propeller and the one on top of it are spinning. The structure in Fig. 3 can be adapted to increase the distance between propellers. The spinning rate of the measured propeller is constant, for the other we have recorded data for the same six different values of the previous setting (see again Fig. 6). Fig. 8 illustrates the measured force. The further the propellers are, the lower the loss in thrust with respect to the one without cross-influence.

The third experimental setting corresponds to a different

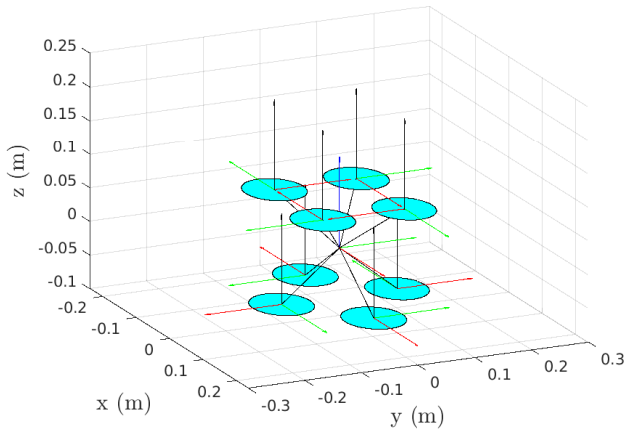

Fig. 9. Twisted configuration of the bottom propellers in the third experimental setup.

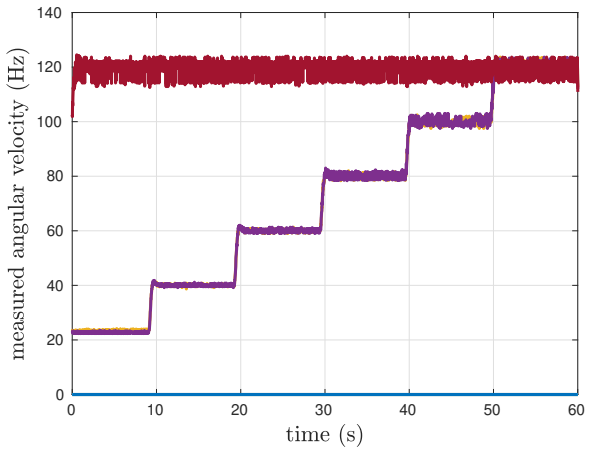

Fig. 10. Measured angular velocity for the experimental set-up in Fig. 9: the measured propeller and the two closest above are spinning. The red signal corresponds to the measured propeller; the blue line at zero to all the others but the two closest above.

configuration of the hosting structure of the propellers. The plane containing the four bottom rotors is rotated by $45°$ around the axis orthogonal to the plane itself, as illustrated in Fig. 9. As in the previous settings, all propellers are pointing up. We focus the data acquisition on the propellers that are expected to contribute the most. Therefore, only the measured propeller and the two closest on top of it are spinning with the measured angular velocities plotted in Fig. 10. Fig. 11 illustrates the measured force. Because the relative position of the top rotors spinning is not aligned with the thrust produced by the measured one, the force generated is not affected twice as much as with the single propeller aligned on top.

The fourth experimental setting corresponds to tilting each propeller of $10°$ around its x−axis starting from the original non-twisted configuration. Fig. 12 illustrates the measured force with all the propellers spinning as shown in Fig. 4.

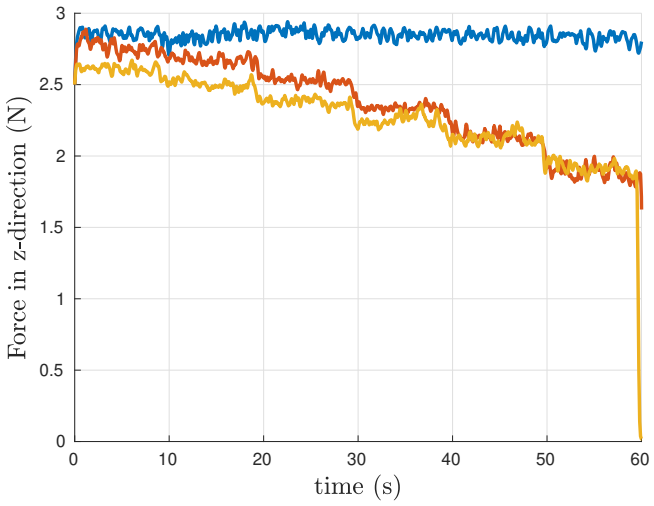

Fig. 11. Measured force in the third experimental set-up with the bottom rotors rotated by $45°$ in yellow. As a reference for the reader we plot also the force without cross-influence (blue) and the force measured in the previous experimental setting, due to the influence of the propeller aligned on top (red).

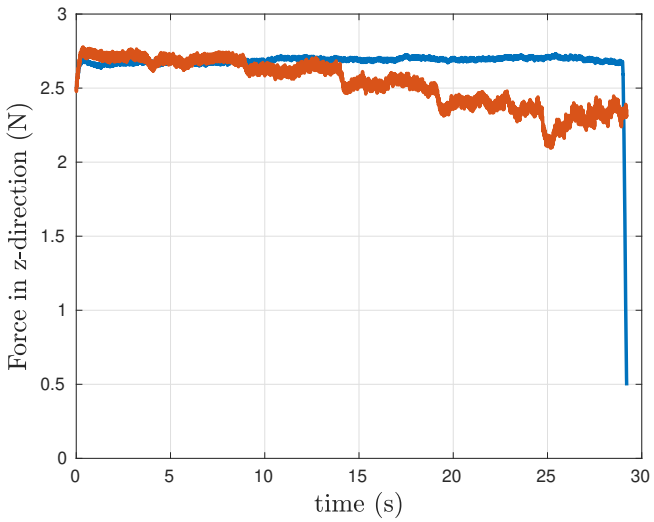

Fig. 12. Measured force in the fourth experimental set-up with all the rotors tilted by $10°$ around their x− axis. As a reference for the reader we plot also the force without cross-influence (blue).

A. *Model fitting on training set*

The proposed model of the thrust coefficient for propeller i is constant for a given set-up of n propellers if the angular velocities and the relative positioning do not change, which is also an approximation of the real phenomenon because external factors could in general cause variations of the coefficient $c_{f,i}$ in time. Hence, we can infer that the force model we assume (1) will predict a thrust value for each configuration $\{\boldsymbol{\omega}_i, \boldsymbol{\omega}_{j=0:n}, \mathbf{p}_{i,j=0:n}\}$, i.e., per each scenario and set of the angular velocities of the propellers. Based on this and because the angular velocity values of all the propellers are measured, we can retrieve from the force measurements a set of experimental c_f's.

For each configuration $\{\boldsymbol{\omega}_i, \boldsymbol{\omega}_{j=0:n}, \mathbf{p}_{i,j=0:n}\}$, we compute the average thrust over the measurements and divide by

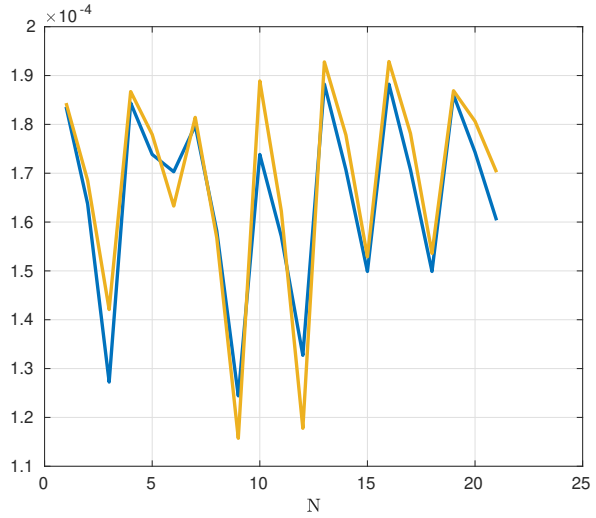

Fig. 13. Estimated $\hat{c}_f$ (yellow) against the experimental c_f (blue) on the training set.

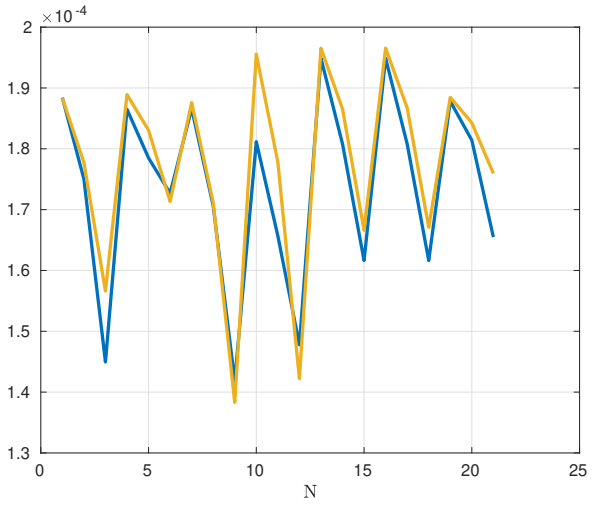

Fig. 14. Estimated $\hat{c}_f$ (yellow) against the experimental c_f (blue) on the testing set.

the squared angular velocity value w_i to get the experimental thrust coefficient c_f that gives the best prediction of the force. Let us indicate as N the number of configurations, each of which corresponds to a value of the experimental thrust coefficient c_f obtained as described above and $\mathbf{c}_f \in \mathbb{R}^N$ the stack of all the experimental coefficients. Without cross-influence, our model boils down to the constant coefficient $c_{f,0}$, whose experimental value is obtained by averaging across all the force measurements with only the measured propeller spinning. Let us indicate as $\mathbf{c}_{f,0} \in \mathbb{R}^N$ the vector $\mathbf{c}_{f,0} = c_{f,0}\mathbf{1}$.

We compute the vector of coefficients $\mathbf{x} = [x_1, x_2, x_3]^T$ by solving the least squares problem:

$$\mathbf{x}^* = \underset{\mathbf{x}}{\operatorname{argmin}} \left[\mathbf{c}_f - \mathbf{c}_{f,0} + \mathbf{A}\mathbf{x} \right] \tag{4}$$

where $\mathbf{A} \in \mathbb{R}^{N\times 3}$ is as tall as the number of experiments and as large as the number of coefficients. One row $\mathbf{a}_k = [a_{0,k}, a_{1,k}, a_{2,k}]$ of $\mathbf{A}$ stores the summations in (3), whose terms are completely known given the experimental setting $\{\boldsymbol{\omega}_i, \boldsymbol{\omega}_{j=0:n}, \mathbf{p}_{i,j=0:n}\}$:

$$\begin{aligned} \mathbf{a}_{0,k} &= \sum_j \frac{{w_j}^2}{|w_i| p_{ij}} \\ \mathbf{a}_{1,k} &= \sum_j \frac{{w_j}^2}{|w_i| p_{ij}} \cos\left(\frac{1}{2}\theta_{p,ij}\right) \\ \mathbf{a}_{2,k} &= \sum_j \frac{w_j^2}{|w_i|} \cos\left(\frac{1}{2}\theta_{p,ij}\right) \cos^2\left(\theta_{w,ij}\right) \end{aligned} \tag{5}$$

After having assembled matrix $\mathbf{A}$, the parameters are computed as $\mathbf{x}^* = \mathbf{A}^\dagger(\mathbf{c}_f - \mathbf{c}_{f,0})$, where $\mathbf{A}^\dagger$ is the Moore-Penrose pseudo-inverse.

Because the experimental settings are designed to observe the different factors contributing to the thrust, we split in two the data acquired in each of them, and use half for training and half for testing. We also take care that each half is representative in terms of angular velocity magnitude. The minimization in (4) will provide a model whose validity holds in a neighborhood of the experimental data used. We encourage the users to consider their typical testing configuration while collecting the training data, keeping in mind that the proposed model holds for small relative orientations. Fig. 13 shows the difference between estimated $\hat{\mathbf{c}}_f = \mathbf{c}_{f,0} - \mathbf{A}\mathbf{x}$ and experimental thrust coefficients on the training dataset.

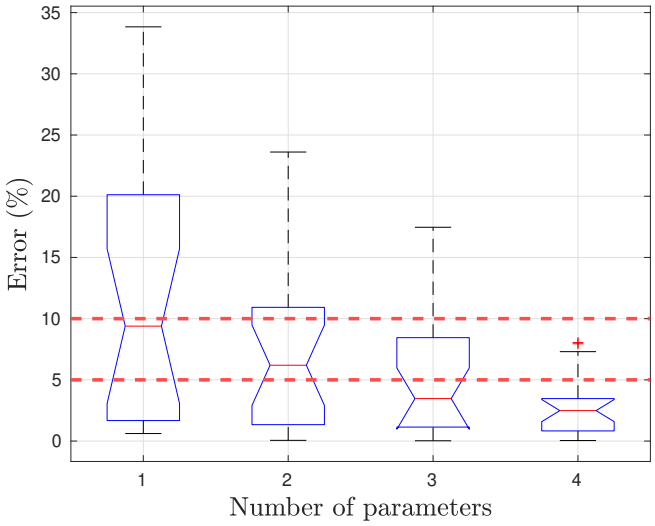

Fig. 15. Boxplot of the percentage error between estimated and experimental thrust force with different models: on the x-axis the number of parameters.

B. Model testing on test set

The optimal set $\mathbf{x}^*$ found on the experimental data as explained in the previous section was used to predict the estimated thrust coefficients applying:

$$\hat{\mathbf{c}}_f = \mathbf{c}_{f,0} - \mathbf{A}\mathbf{x}^* \tag{6}$$

Recall that $\mathbf{c}_{f,0}$ are the experimental influence-free coefficients and the matrix $\mathbf{A}$ is computed according to (5) based on the current experimental setting $\{\boldsymbol{\omega}_i, \boldsymbol{\omega}_{j=0:n}, \mathbf{p}_{i,j=0:n}\}$.

Fig. 14 shows the difference between estimated $\hat{\mathbf{c}}_f = \mathbf{c}_{f,0} - \mathbf{A}\mathbf{x}^*$ and experimental thrust coefficients on the test dataset. The estimated thrust coefficients can consistently approximate the experimental ones in all the experiments, giving a mean percentage error of 2.8% and a maximum of 8.0%. The same accuracy is achieved in predicting the thrust force, as illustrated in Fig. 15.

Such a good approximation is obtained by adding the cross-influence effect in the model, which we do by using four parameters instead of the single coefficient used in the literature [6]. The proposed model has just the right complexity to predict the force and the thrust coefficient (see Fig. 15) with a mean error lower than 5% and a maximum error lower than 10%. To show this, we fitted and tested models with fewer parameters. In the design of such models, we keep in mind that all the three main factors, i.e., p_{ij}, $\theta_{w,ij}$, $\theta_{p,ij}$., should be taken into account.

The three-parameters model we tested is:

$$c_{f,i} = c_{f,0} - \frac{w_j^2}{|w_i|} \sum_j \left[\frac{x_1}{p_{ij}} + \frac{x_2}{p_{ij}} \cos\left(\frac{1}{2}\,\theta_{p,ij}\right) \cos^2\left(\theta_{w,ij}\right) \right] \tag{7}$$

where the first term is the same as in (3) while the second fuses the contributions of the second and third terms of (3). With a mean percentage error of 5.5% and a maximum of 17.5%, it can match the mean error requirement but not the maximum one.

The two-parameters model is instead:

$$c_{f,i} = c_{f,0} - \frac{w_j^2}{|w_i|} \sum_j \left[\frac{x_1}{p_{ij}^2} \cos\left(\frac{1}{2}\,\theta_{p,ij}\right) \cos^2\left(\theta_{w,ij}\right) \right] \tag{8}$$

In this case, the single coefficient x_1 in the summation multiplies the product of all the relevant quantities in the description of cross-influence between propellers i and j. With a mean percentage error of 8.1% and a maximum of 23.6%, it can match neither the mean error requirement nor the maximum one.

The one-parameter model is $c_{f,i} = c_{f,0}$ that cannot predict the force in the presence of cross-influence giving the worst results, with a mean percentage error of 12.0% and a maximum of 33.8%.

V. Conclusion

In this paper, we presented a novel model of the thrust coefficient of a propeller, that takes into account the cross-influence between propellers that occurs in multi-rotor UAVs and typically reduces the thrust of some of them, the rotational speed being equal. Our method improves significantly the prediction of the force generated by a set of propellers in MAVs, which can be used in power consumption analysis. This comes at the expense of a larger set of parameters, four, and a more complex model taking into account the relative positioning and the angular velocities of the interacting rotors. We believe that this small additional complexity is totally acceptable in practice. We give a physical intuition of the proposed model based on the aerodynamic mechanisms and present experimental procedure and data that we used to fit and validate the model.

Future work includes enriching the training and test data with larger relative orientations. Investigation and data fitting on that will lead to a more general model. In addition, we can use the enriched dataset to validate a modified model of the thrust coefficient that makes it positive by construction. Moreover, we plan to propose an analogous model for the torque coefficient c_τ that is also affected by cross-influence effects. Finally, we plan to present a use-case example on a platform, to illustrate how the wrench map changes with the proposed adaptive model.

References

[1] Mohamed Ghazali, Yasser Bouzid, Saddam Hocine Derrouaoui, and Mahmoud Belhocine. Optimal PID control of a novel multirotor with inclined rotors and spatial configuration. In *2023 International Conference on Networking and Advanced Systems (ICNAS)*, pages 1–6, 2023.

[2] Dario Brescianini and Raffaello D'Andrea. Design, modeling and control of an omni-directional aerial vehicle. In *2016 IEEE International Conference on Robotics and Automation (ICRA)*, pages 3261–3266, May 2016.

[3] Sangyul Park, Jeongseob Lee, Joonmo Ahn, Myungsin Kim, Jongbeom Her, Gi-Hun Yang, and Dongjun Lee. ODAR: Aerial Manipulation Platform Enabling Omnidirectional Wrench Generation. *IEEE/ASME Transactions on Mechatronics*, 23(4):1907–1918, August 2018. Conference Name: IEEE/ASME Transactions on Mechatronics.

[4] Giulia Michieletto, Markus Ryll, and Antonio Franchi. Fundamental actuation properties of multirotors: Force–moment decoupling and fail–safe robustness. *IEEE Transactions on Robotics*, 34(3):702–715, 2018.

[5] Elgiz Baskaya, Mahmoud Hamandi, Murat Bronz, and Antonio Franchi. A novel robust hexarotor capable of static hovering in presence of propeller failure. *IEEE Robotics and Automation Letters*, 6(2):4001–4008, 2021.

[6] Youssef Aboudorra, Chiara Gabellieri, Ralph Brantjes, Quentin Sablé, and Antonio Franchi. Modelling, analysis, and control of omnimorph: an omnidirectional morphing multi-rotor uav. *Journal of Intelligent & Robotic Systems*, 110(1):21, 2024.

[7] Mike Allenspach, Karen Bodie, Maximilian Brunner, Luca Rinsoz, Zachary Taylor, Mina Kamel, Roland Siegwart, and Juan Nieto. Design and optimal control of a tiltrotor micro-aerial vehicle for efficient omnidirectional flight. *The International Journal of Robotics Research*, 39(10-11):1305–1325, September 2020. Publisher: SAGE Publications Ltd STM.

[8] Mahmoud Hamandi, Federico Usai, Quentin Sablé, Nicolas Staub, Marco Tognon, and Antonio Franchi. Design of multirotor aerial vehicles: A taxonomy based on input allocation. *The International Journal of Robotics Research*, 40(8-9):1015–1044, 2021.

[9] Sangyul Park, Jongbeom Her, Juhyeok Kim, and Dongjun Lee. Design, modeling and control of omni-directional aerial robot. In *2016 IEEE/RSJ International Conference on Intelligent Robots and Systems (IROS)*, pages 1570–1575, October 2016. ISSN: 2153-0866.

[10] Mahmoud Hamandi, Kapil Sawant, Marco Tognon, and Antonio Franchi. Omni-Plus-Seven (O7+): An Omnidirectional Aerial Prototype with a Minimal Number of Unidirectional Thrusters. In *2020 International Conference on Unmanned Aircraft Systems (ICUAS)*, pages 754–761, September 2020. ISSN: 2575-7296.

[11] Markus Ryll, Davide Bicego, and Antonio Franchi. Modeling and control of FAST-Hex: A fully-actuated by synchronized-tilting hexarotor. In *2016 IEEE/RSJ International Conference on Intelligent Robots and Systems (IROS)*, pages 1689–1694, October 2016. ISSN: 2153-0866.

[12] Mina Kamel, Sebastian Verling, Omar Elkhatib, Christian Sprecher, Paula Wulkop, Zachary Taylor, Roland Siegwart, and Igor Gilitschenski. The Voliro Omniorientational Hexacopter: An Agile and Maneuverable Tiltable-Rotor Aerial Vehicle. *IEEE Robotics & Automation Magazine*, 25(4):34–44, December 2018. Conference Name: IEEE Robotics & Automation Magazine.

[13] Alex Zanotti and Davide Algarotti. Aerodynamic interaction between tandem overlapping propellers in evtol airplane mode flight condition. *Aerospace Science and Technology*, 124:107518, 2022.

[14] Reynard de Vries, Nando van Arnhem, Tomas Sinnige, Roelof Vos, and Leo L.M. Veldhuis. Aerodynamic interaction between propellers of a distributed-propulsion system in forward flight. *Aerospace Science and Technology*, 118:107009, 2021.